ISSN 0006-3509, Biophysics, 2009, Vol. 54, No. 1, pp. 10–22. © Pleiades Publishing, Inc., 2009.
Original Russian Text © G.Yu. Riznichenko, N.E. Belyaeva, I.B. Kovalenko, A.B. Rubin, 2009, published in Biofizika, 2009, Vol. 54, No. 1, pp. 16–33.

CELL BIOPHYSICS

Mathematical and Computer Modeling of Primary Photosynthetic Processes

G. Yu. Riznichenko, N. E. Belyaeva, I. B. Kovalenko, and A. B. Rubin

Biological Faculty, Moscow State University, Moscow, 119992 Russia
e-mail: riznich@biophys.msu.ru

Received August 20, 2008

Abstract—We review the recent research on kinetic and direct multiparticle modeling of the processes in the photosynthetic membrane conducted at the Chair of Biophysics of the Biological Faculty, Moscow State University. The models take into account the modern experimental data on the heterogeneous structure and the kinetic characteristics of the system. The generalized kinetic model describes the processes in multisubunit complexes (photosystems I and II, the cytochrome complex), the coupled transmembrane ion fluxes and generation of the electrical and electrochemical potentials. Identification of the model parameters allows estimation of the rate constants for reactions that cannot be examined experimentally. Multiparticle models provide a vivid picture of the interaction between the electron transport chain components in the thylakoid lumen and stroma, and explicitly represent Brownian diffusion and electrostatic interactions between electron carriers. Combination of different description methods (differential equations and the Brownian dynamics formalism) makes it possible to model, in the complicated 3D environment of the plant cell, the processes that in the aggregate ensure the high efficacy of energy transduction in photosynthesis.

Key words: photosynthesis, primary processes, kinetic modeling, simulation modeling

DOI: 10.1134/S0006350909010035

INTRODUCTION

The photosynthetic membrane, which harbors electron transport (ET) and coupled processes whereby light energy is stored in the transmembrane potential and chemical bonds (Fig. 1), is one of the best-studied subcellular systems. In recent years, vast data have been accumulated on the molecular structure of photosynthetic reaction centers (RC), ATP synthase and other complexes involved in energy transduction, as well as on the geometry of the intracellular nanostructures supporting the efficacy of these processes. Mathematical and computer models permit integration of the knowledge on separate components of the system and expedient study of the mechanisms regulating the photosynthetic processes.

The possibility of directly monitoring the redox conversions of separate components (by spectrophotometry, EPR, etc.) upon a light stimulus allows correct statement of the problem of identifying the model parameters from kinetic data. This is a major advantage of the photosynthetic system over most metabolic networks, where the dynamics of individual metabolites cannot be monitored so that model building is largely phenomenological.

The works of the 1980–90s on modeling and parameter identification for processes in isolated PS I and PS II complexes and bacterial RC have revealed an essential difference in the regulation of the reactions within the complexes and the entry/egress reactions [1–4].

Experiments with various RCs have shown that these evolutionarily optimized systems maintain their structural and functional organization upon isolation by different means and over a broad range of external influences, from which they are shielded by their protein/lipid surroundings. Absorption of a light quantum entails charge separation in the primary photoactive pair and is attended by conformational changes in the RC components that prevent back ET and loss of energy through fluorescence. Within the complex, the reaction rates depend on illumination intensity. Excessive illumination activates dissipative radiationless processes; the contribution of the latter is one of the tasks of mathematical modeling.

A different type of regulation is observed for the steps where ET involves mobile carriers: plastoquinone PQ between PS II and the cytochrome complex, plastocyanin Pc between the cytochrome complex and PS I, ferredoxin Fd at the stromal side of PS I. In the native thylakoid, the kinetic parameters of such steps are determined by the number of these interactions, i.e. by

Abbreviations: Chl, chlorophyll; ET, electron transport; Fd, ferredoxin; Fld, flavodoxin; Pc, plastocyanin; PQ, plastoquinone; PS, photosystem; RC, reaction center.

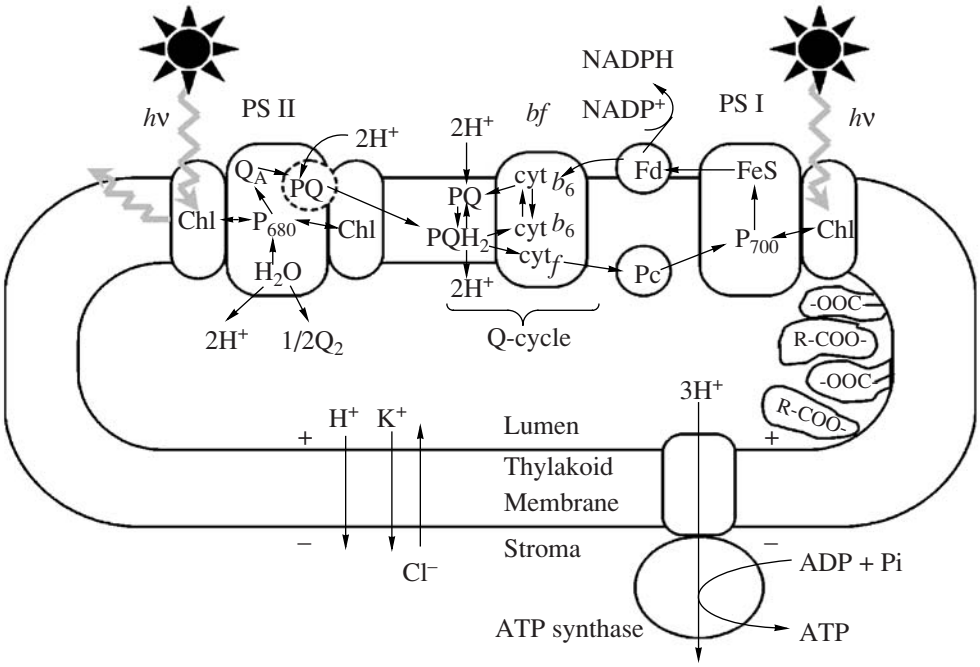

Fig. 1. General scheme of processes considered in the integrated model. PS are the photosystems, *bf* is the cytochrome complex, Chl is the antennal chlorophyll, PQ is plastoquinone, (PQH_2, plastoqinol), Fd is ferredoxin, Pc is plastocyanin; $R\text{-}COO^-$ are buffer groups. Plus and minus signs denote light-induced charging; wavy lines denote fluxes of absorbed quanta and fluorescence, black arrows show electron and ion fluxes.

the time of diffusion of the carrier to the complex and the probability of its docking in the proper site (largely determined by local electrostatic interactions). Besides the diffusion parameters for PQ in the membrane, Pc in the lumen, Fd in the stroma, very important is the geometry of the reaction volume. The rate constants for these steps may change by several orders of magnitude upon varying the external conditions, and these are the points of action of regulatory factors such as viscosity, pH, endogenous inhibitors, metabolites, etc. Modeling of various processes within a unified system of primary photosynthetic processes requires a panoply of mathematical and computer approaches.

Numerous models have been proposed for the processes in PS I [5–9] and PS II [10–26]. The recent models [16–20, 24–26] provide a detailed description of ET comprising tens of differential equations. The main attention of researchers is attracted to the initial part of the fluorescence induction curve. Indeed, in this respect the PS II models yield good results at high illumination and relatively short times (within 1 s). However, to study the regulation of primary photosynthetic processes by the cell metabolic systems we need models covering the aggregate of processes in the thylakoid membrane.

Such models developed over the last decade at the Chair of Biophysics of the Biological Faculty, Moscow State University include a generalized kinetic model [2, 3, 27, 28] and a set of direct miltiparticle computer simulation models [4, 29–32]. Here we consider their basic features, main results, and prospects.

KINETIC MODEL OF A PHOTOSYNTHETIC MEMBRANE

The processes described in the model are shown in Fig. 1. We have analyzed the models of ET in isolated PS II [11, 14, 26, 33], PS I [6–9], and cytochrome complexes [34]. The generalized model [2–4, 27, 28] also considers the transmembrane ion fluxes, oxygen evolution, generation of membrane potentials, ATP synthase activity, and the role of buffer groups in the stromal and lumenal spaces.

ELECTRON TRANSFER IN MULTISUBUNIT COMPLEXES

The basic elements of the photosynthetic ET chain are the membrane-embedded pigment–protein complexes of PS I and PS II, whereby the energy of absorbed light quanta is used for charge separation, and the cytochrome complex whereby ET is coupled with transmembrane proton transfer, i.e. generation of the electrochemical potential used by ATP synthase (see Fig. 1.)

Within the complexes, ET follows a fixed path, and the complex operates as a unity. The catalytic cycle for every complex can be represented as a set of possible states, determined by the number of the constituent

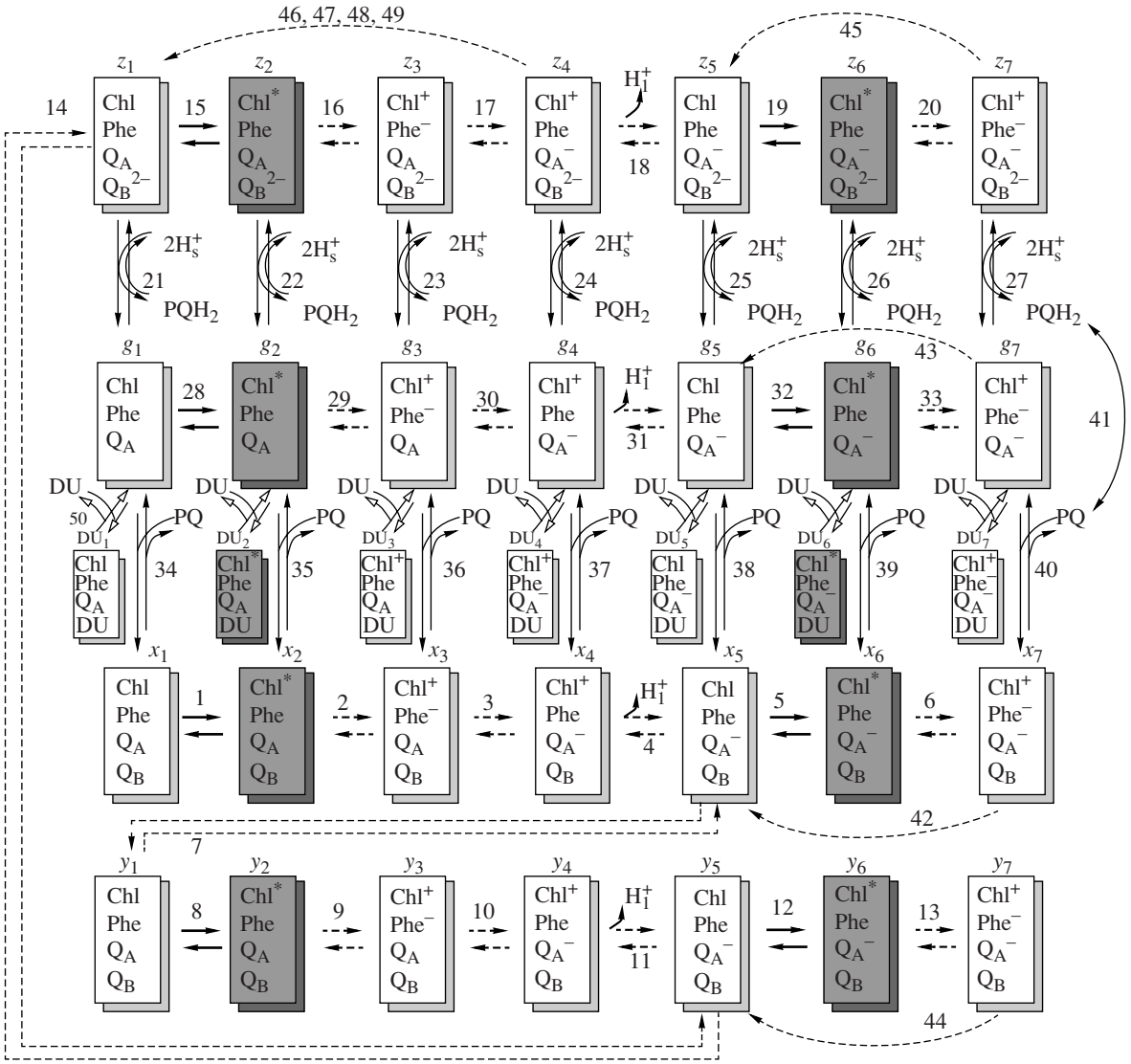

Fig. 2. Scheme of the PS II catalytic cycle. Each rectangle represents a kinetic state defined by the redox states of constituent electron carriers. Shaded are emission-competent states. Chl unites antennal pigments and RC P680; Phe is the primary acceptor pheophytin; Q_A and Q_B are quinone acceptors; subscripts mark protons (L) released into lumen and (S) absorbed from stroma. Dashed arrows mean fast steps (characteristic times <0.1 ms), solid arrows mean slow steps (at least 1 ms), thick arrows denote light stages. Number at the arrows enumerate reactions; designation above the rectangles (x_i, y_i, z_i, g_i, du_i, $i = 1, \ldots, 7$) indicate model variables. The row of smaller rectangles pertains to states with inhibitor diuron DU) occupying the Q_B site and precluding ET between primary and secondary quinones. Dashed arcs denote nonradiative recombination: $Phe^-/P680^+$ (42–45), $Q_A^-/P680^+$ (46–49).

electron carriers and the number of possible states of each carrier (oxidized, neutral, reduced, excited, protonated, etc.). In our models, intracomplex ET is described by sets of ordinary differential equations (ODE) where the variables are the probabilities of these states and the parameters are the rate constants for transitions between the states.

The question of describing ET within complexes has been raised in [35, 36] and elaborated upon in [37]. In a series of works of our Chair, this approach was applied to isolated PS I and II complexes and bacterial RC [1, 5–8, 38–40].

Let a multienzyme complex

$$\longrightarrow [C_1 C_2 \ldots C_n] \longrightarrow \quad (1)$$

include n electron carriers, each of which can have a finite number of states. The scheme of transitions between states is a graph where the nodes represent possible states and the edges (with arrows) represent the transitions; such graphs are exemplified in Figs. 2–5.

The transitions can be described with ODE for state probabilities

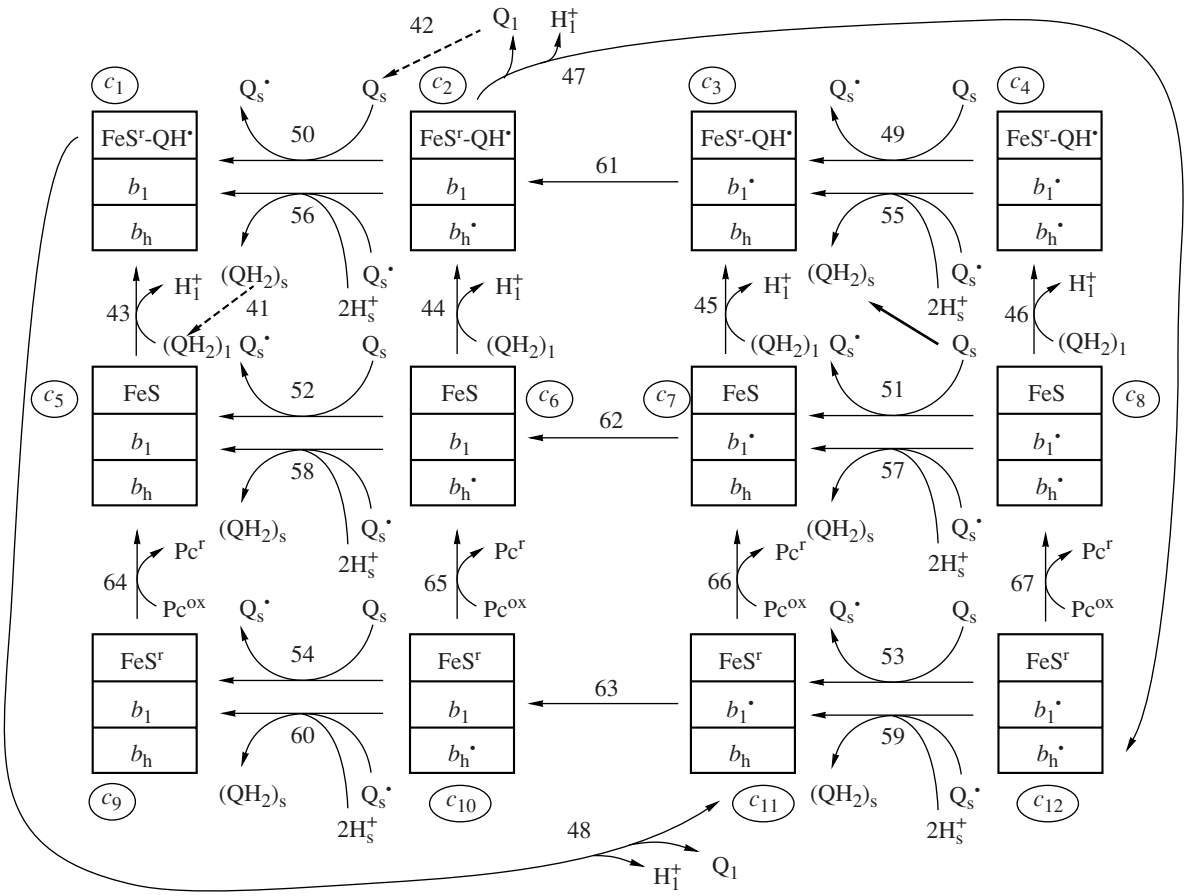

Fig. 3. Scheme of the catalytic cycle of the cytochrome complex. Each rectangle represents a kinetic state defined by the redox states of constituent electron carriers. The *bf* module operates in the Q cycle. Upon reduction by PS II, PQH_2 diffuses in the membrane (42) and is oxidized in the lumenal site of the *bf* complex, whereby one electron goes to the Rieske FeS center (high-potential path) and the other to oxidized b_l (low-potential path). Electrogenic steps were assumed to be the release of two protons to the lumen (43–48), uptake of two protons from the stroma (55–60), and transmembrane ET b_l–b_h (61–63). Model variables are designated in ovals. Superscripts denote reduced and oxidized forms.

$$\frac{dp_i}{dt} = \sum_{j=1}^{l} (p_j k_{ji} - p_i k_{ij}) \qquad (2)$$

Here p_i is the probability of the complex being in the i-th state, k_{ij} is the rate constant for transition from the i-th to the j-th state. Summed is the difference between the probability of transition to i from other states (positive) and the probability of transition from i to other states (negative). The initial values are given as $p_i(0) = b$, $i = 1, \ldots, l$ or in vector form

$$\frac{dP}{dt} = K^T P, \quad P(0) = B \qquad (3)$$

The probability of finding carrier q in state G appears as

$$P(G) = \sum_{S_q \in G} p(S_q, t), \qquad (4)$$

with summation over all states S_q where the q-th component is in state G.

The probabilities for k_{ij} transitions are not constant values, they depend on the state of the whole complex (conformation, granal/stromal localization, etc.) and on other variables and parameters (temperature, membrane potential, external electric field, etc.). In our kinetic models, special attention is paid to the dependence of transition rate constants on the photoinduced electrical potential.

PHOTOSYSTEM II COMPLEX

There are many works where the models of PS II events are used to describe the kinetics of fluorescence rise upon switching on continuous illumination (the so-called O-J-I-P kinetics). These models consider in detail the ET in PS II, the interaction with antennal Chl, and the processes in the water-splitting complex [16–21, 24, 25, 41]. Therewith, fluorescence intensity is

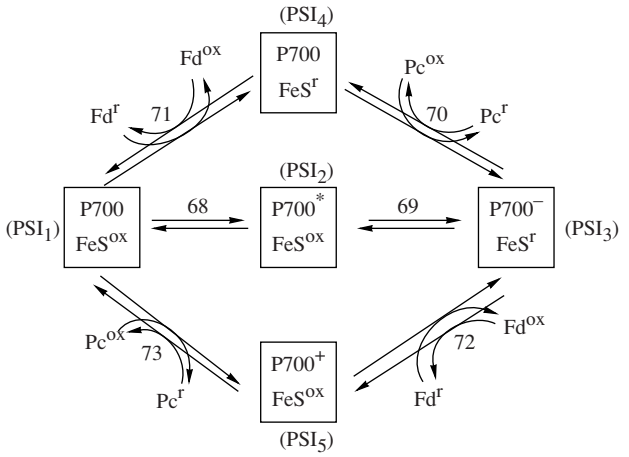

Fig. 4. Simplified scheme of PS I processes. Designations as in Figs. 1–3.

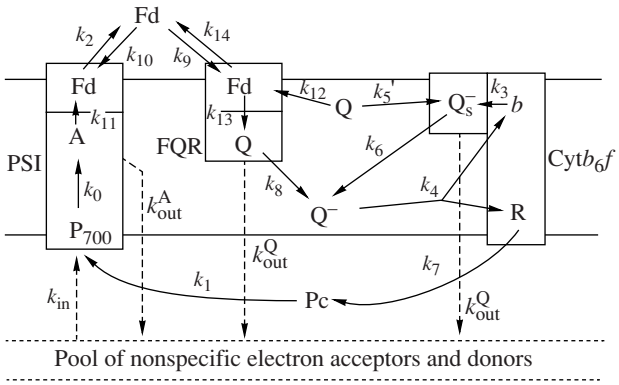

Fig. 5. Scheme for the kinetic model of cyclic electron transport around photosystem I. Boxes stand for PS I, FQR, and cytochrome b_6/f complexes; P_{700}, pigment of the PS I reaction center; *A*, generalized acceptor; *R*, Rieske center; *b*, high-potential cytochrome b_h; Fd, ferredoxin; Pc, plastocyanin; Q, plastoquinone; Q^{--}, plastoquinol; Q_n, semiquinone at the *n*-th site of the cytochrome complex (on the outer side of the membrane). Arrows indicate ET k_{in}, k_{out}, k_1, …, k_{13}, and k_{14} are the rate constants for the respective reactions. Dashed lines depict the boundaries of the thylakoid membrane and the boundary of the pool of nonspecific electron acceptors and donors.

usually taken to be proportional to the concentration of closed RC. Comparison of the models where fluorescence is a function of acceptor levels [Q_A^-] or [Phe^-] suggests [21] that they all describe the O-J-I-P kinetics with reasonable accuracy (2%).

The distinction of our model is that we do not introduce for fluorescence any function of model variables, but take it to be proportional to the concentration of excited Chl, i.e. its physical source.

Figure 2 shows the version of state scheme [26] used to model the processes in a native chloroplast and in the presence of an inhibitor diuron (row of small rectangles). For detailed consideration of particular experimental situations, the scheme can be modified.

Each PS II state in the scheme includes four components: Chl P680, pheophytin Phe, one-electron quinone carrier Q_A, and a binding site for the secondary acceptor Q_B.

We assume that the excitation energy (light quantum absorbed by an antennal Chl molecule) is rapidly (in picoseconds) distributed over the entire PS II Chl pool including the RC P_{680}. The Chl component can be neutral (Chl), excited ($Chl^•$), or oxidized (Chl^+). Each one-electron acceptor can be neutral (Phe, Q_A) or reduced (Phe^-, Q_A^-).

The PQ binding site can be empty (2nd row) or can contain neutral PQ (Q_B, 4th row) as well as carry one (Q_B^-, 5th row) or two electrons (Q_B^{2-}, 1st row in Fig. 2). Thus, the states corresponding to particular rows x_i, y_i, z_i, g_i (i = 1, 2, …, 7) differ in the bound PQ state. Detailed description of transitions between PS II states is given elsewhere [14, 26].

Formation of the excited Chl state is determined by the "light constants" $k_L = k_i$, i = 1, 5, 8, 12, 15, 19, 28, 32 proportional to illumination intensity. Fluorescence is set by $k_F = k_{-i}$; the fluorescence yield is calculated as the product of k_F/k_L by the sum of fluorescing states

$$F = \frac{k_F}{k_L}(x_2 + y_2 + z_2 + g_2 + x_6 + y_6 + z_6 + g_6) \qquad (5)$$

The additional row of small rectangles in Fig. 2 represent states where the Q_B site is occupied by diuron (variables DU_i), precluding ET to mobile PQ and further to the cytochrome complex and PS I.

The PS II model was used as a part of the generalized model [27, 28] and as an autonomous model to describe the rapid phase of fluorescence induction (within 1 s after switching on intense illumination) [14, 33, 42].

This model also proved expedient for experimental situations when the connection of PS II with further ET was blocked or negligible, and the changes in the electrochemical potential could be disregarded. Thus works [33, 43] present fitting to the data on fluorescence excited by a saturating 10-ns pulse over the time interval from 100 ns to 10 s in preparations of a thermophilic unicellular green alga *Chlorella pyrenoidosa* Chick (experiments of G. Renger's lab in Berlin). Thereby we could estimate the rate constant for reactions that cannot be followed experimentally, and assess the relation of energy fluxes in PS II. These works show the necessity of considering the nonradiative energy dissipation, which is essential under intense illumination.

THE CYTOCHROME *bf* COMPLEX

The cytochrome complex is a major component of the photosynthetic chain, connecting PS II and PS I; it is a "checkpoint" both for the linear ET from the water-splitting complex to the terminal acceptors and for the cyclic ET around PS I [44]. Its important function is to couple the electron flow with the transmembrane potential by regulating the proton transfer by the quinone pool. The scheme of our submodel [34] for the cytochrome complex is shown in Fig. 3.

Each state (rectangle) includes the Rieske iron-sulfur center (FeS_R) and two Cyt *b* hemes—high-potential b_H and low-potential b_L, each of which can be neutral or reduced. The paper [34] gives a detailed description of the model and the results of modeling and parameter identification from the experimental data [45] on the redox conversions of b_H, reduction of the acceptor Pc, and associated pH changes.

THE ROLE OF THE ELECTROCHEMICAL POTENTIAL

The processes of electron and ion transfer give rise to a transmembrane potential, which in turn influences the electron fluxes [46]. Multiple experiments with external fields confirm that the ET rate within the complex depends on the thylakoid membrane potential [47, 48].

Describing the electron movement across the photosynthetic membrane, it is necessary to take into account the dependence of its rate on the potential difference $\Delta\Psi$. In our models, $\Delta\Psi$ is a dynamic variable, changing with the overall charge at the lumenal and the stromal sides of the membrane [49]:

$$\frac{c_m}{F}\frac{d(\Delta\Psi)}{dt} = \upsilon(q_{lumen}) - \upsilon(q_{stroma})$$

where c_m is membrane capacity, F is Faraday constant, $\upsilon(q_{lumen})$, $\upsilon(q_{stroma})$ are the respective charge volume densities, q_{lumen}, q_{stroma} are functions of the respective $[H^+]$, $[K^+]$, $[Cl^-]$ which are model variables.

The electrogenicity of each particular step of charge transfer was evaluated as [50, 51]

$$\begin{aligned} k_j(\Delta\psi) &= k_j^0 \exp(\delta\beta_j F\Delta\psi/2RT), \\ k_{j-}(\Delta\psi) &= k_{j-}^0 \exp(-(1-\delta)\beta_j F\Delta\psi/2RT) \end{aligned} \quad (6)$$

Here superscript (0) pertains to the rate constant at $\Delta\psi = 0$; β_j gives the contribution of each step into $\Delta\psi$; δ is the part of the overall potential that affects the rate of the direct reaction.

The potential–rate dependence is an important property of the models, providing additional possibilities of model verification from experiments on recording the potential under light [52].

PHOTOSYSTEM I COMPLEX

The extent of detail in our model descriptions of PS I depended on the goal of modeling. For the fluorescence induction curves [27] we used a simplified version displayed in Fig. 4.

In the kinetic modeling of the biphasic reduction of P700 in isolated pea chloroplasts with diuron (connected with Fd-dependent cyclic ET), the parameters were identified from the photoinduced EPR 1 signals using a more detailed scheme (Fig. 5) [9].

ELECTRON TRANSPORT BY MOBILE CARRIERS IN THE KINETIC MODEL

In each compartment of the system, ET between complexes is performed by a special carrier: Pc within the thylakoid lumen, Fd in the outer stromal space, and PQ (neutral or doubly protonated) within the membrane lipid bilayer. In the kinetic models, the interaction of the carrier with the complex was described with the conventional apparatus (equations of mass action).

ION TRANSPORT AND BUFFER PROPERTIES

Proton leakage and potential-related ion transport were described with the three-barrier formalism [53, 54]. The same approach was used for ATP synthase.

To describe the buffer properties of the thylakoid lumen and stroma, we assumed three types of buffer group with pK relative to proton ranging 4–8. The dissociation constants were chosen in accordance with the experimental data on thylakoid buffer capacity [55].

PARAMETER VALUES

The model contains tens of parameters, and determination thereof is a separate problem. The choice of parameter values is discussed in the original papers. For the rate constants of ET within the complexes, there are numerous experimental estimates, most of which pertain to isolated complexes illuminated with a powerful short flash, often in the presence of inhibitors. The averaged values were taken as initial ones for our models, and often refined upon fitting. Less studied are the interactions of complexes with mobile carriers, and these data are contradictory. The broad range of literature data is associated with the variability of the geometry of the lumenal and the stromal space, pH, ionic strength, etc. Some parameters of this kind were averaged over a large volume of experimental values, others were varied for the best fit. The corresponding values are listed in tables [26–28, 34]. Estimation of certain parameters required special experiments. For example, the rate constants for dissipative processes in PS II were based on the data on fluorescence yield upon a short powerful light flash [26].

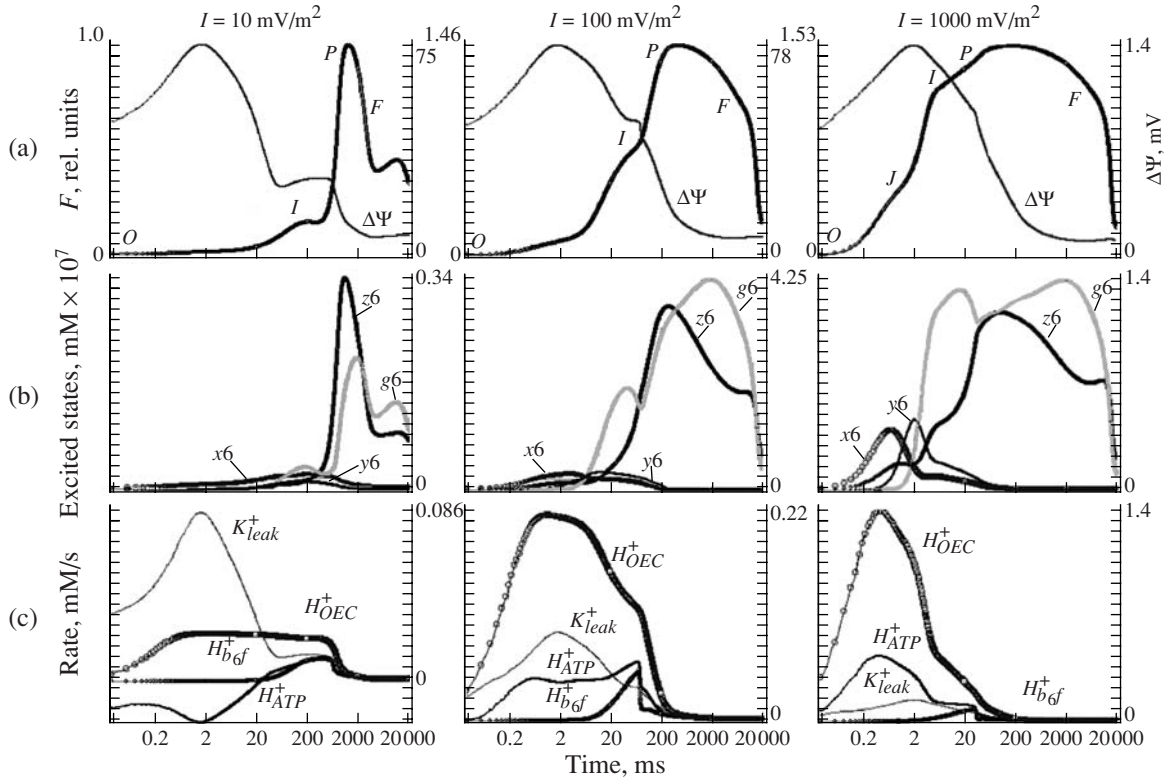

Fig. 6. Induction effects calculated with the proposed model for three illumination levels specified above each column. The time scale is logarithmic. Panels (a), relative fluorescence yield (F) and transmembrane electric potential ($\Delta\Psi$). Panels (b), concentrations of PS II excited states. Panels (c), rates of processes producing and consuming the electric charge in the thylakoid lumen: H^+_{bf} is the proton influx from plastoquinol oxidation at the *bf* lumenal side, H^+_{OEC} is the proton influx from the oxygen-evolving complex; H^+_{ATP} is proton consumption in the ATP synthase reaction; K^+_{leak} is potassium leakage through the membrane.

RESULTS OF MODELING

The thylakoid model allows envisioning the kinetics of variables at different parameter values and initial conditions corresponding to different experimental conditions. Therewith the model provides time curves both for experimentally measurable quantities (fluorescence induction, electrical potential, redox conversions of P700) and for those that are not experimentally observable.

Figure 6 displays the curves generated in the generalized kinetic model for three values of the light constant (high, medium, and low illumination).

Figure 7 shows the experimental scheme and the results of fitting, whereby we could estimate the rate constant for nonradiative dissipation including nonphotochemical quenching associated with the oxidized photoactive P680 and carotenoids (for details, see [26, 43]).

To sum, the kinetic models allow testing the adequacy of our notions on the mechanisms of particular segments of the photosynthetic chain, as well as assessing the contribution of various processes to the kinetic induction curves and the relation of electron fluxes at separate ET steps. Identifying the model parameters from the aggregate experimental data, one can estimate the kinetic parameters that are not yet amenable to experimental determination.

LIMITATIONS OF KINETIC MODELS

The ODE-based kinetic models imply homogeneous distribution of the components. Thus it is assumed that PS I, PS II, and cytochrome complexes are uniformly spread through the membrane, and their interaction with mobile carriers obeys the law of mass action. This mathematical apparatus permits detailed enough description of the events in RC, but it is hardly suitable for ascertaining the role of the spatial organization of the photosynthetic machinery in the regulation of the photosynthetic processes. The geometrical peculiarities and the properties of the milieu where the carriers move can be taken into account by the kinetic models only indirectly, through effective parameter values.

A large number of recent works have been devoted to the heterogeneous structure of the photosynthetic membrane. Electron microscopy testifies to dense posi-

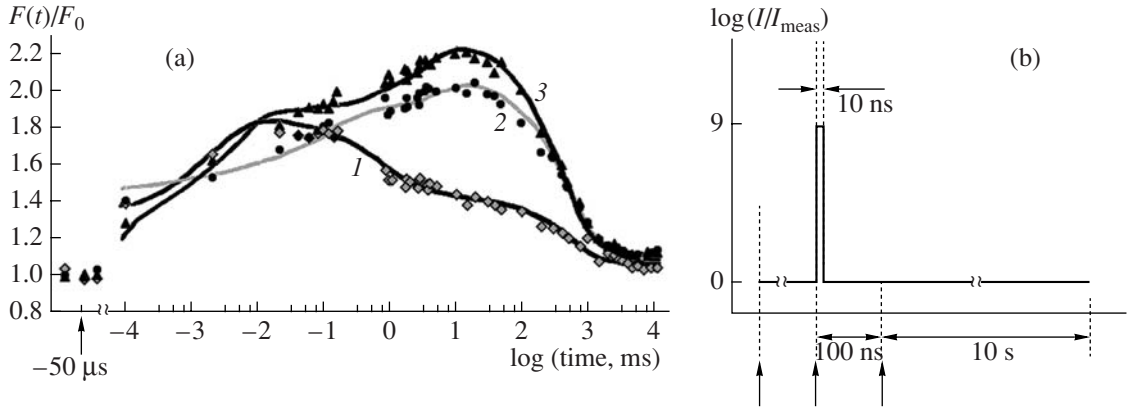

Fig. 7. (a) Experimental data (points) and model curves (lines) for fluorescence induced by a high-power nanosecond pulse (k_L = $6 \cdot 10^8$ s^{-1}) under weak measuring light (k_L = 0.6 s^{-1}); conditions correspond to a native specimen (rhombi, *1*) and inhibition with diuron (circles, *2*) or *o*-phenanthroline (triangles, *3*). (b) Illumination and measuring scheme.

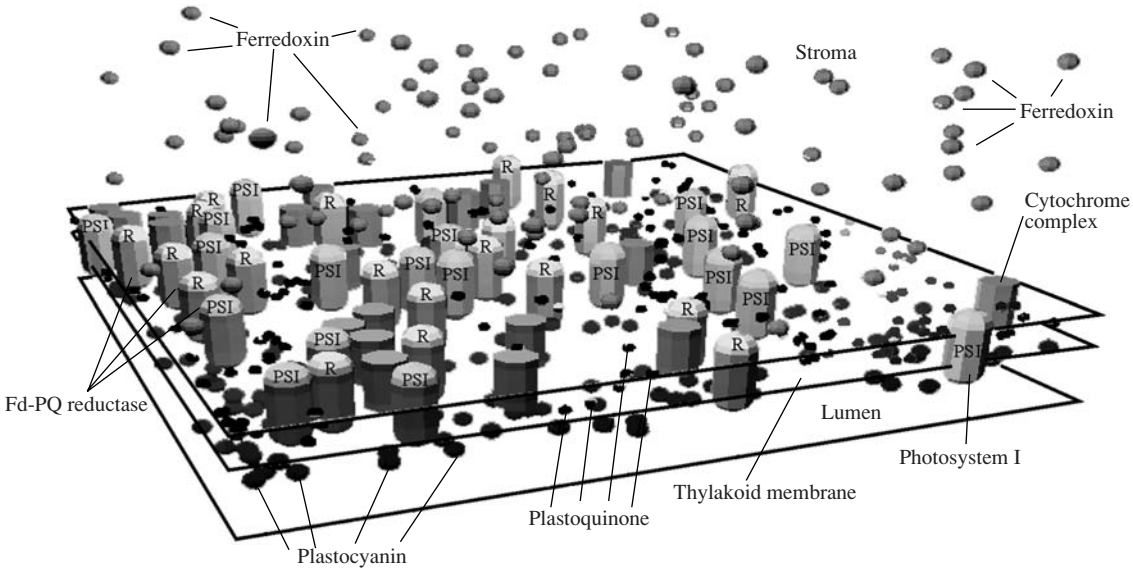

Fig. 8. The 3D stage of the direct multiparticle model.

tioning of the membrane complexes that precludes free intramembrane diffusion of PQ. The available data [45, 56, 57] show that the complexes protrude into the lumen so considerably that the movement of Pc would be hindered. Diffusion in the stromal space also cannot be a priori regarded as unrestricted.

This demonstrates the shortcomings of kinetic modeling which implies homogeneity and free diffusion.

The specific features of the heterogeneous organization of the photosynthetic machinery can be described with direct multiparticle computer models developed over the last five years at the Chair of Biophysics, Biological Faculty together with the Chair of Computer Physics, Physical Faculty of the MSU [4, 9, 29–32]. The possibility of building such models for processes in subcellular nanostructures is due to the recent vigorous development of information technologies, great expansion of computational resources, advances in object-oriented software design and visualization techniques. Apart from the kinetic characteristics that can be obtained with a conventional model, direct simulation provides a 3D visual representation of the system dynamics on different spatiotemporal scales, and enables one to monitor individual components as well as obtain statistical knowledge.

THE STAGE AND PARTICIPANTS OF THE DIRECT SIMULATION MODEL

The model can be envisaged as a 3D stage comprising the thylakoid membrane, the lumen, and the stromal space (Fig. 8). The stage harbors oligoenzyme PS and cytochrome complexes (fixed in this version) and

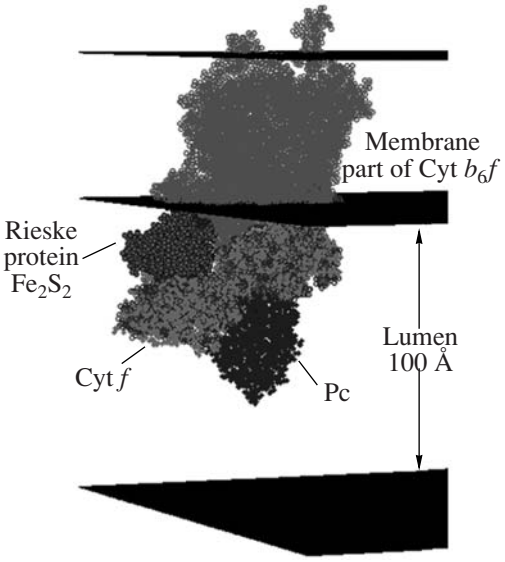

Fig. 9. The arrangement of the Pc-Cyt *f* complex on the membrane-embedded *bf*, obtained by combining the PDB structures 2PCF and 1Q90.

mobile carriers PQ, Pc, Fd. The algorithm generating the stage has been described elsewhere [58].

The motion of Pc, Fd, and PQ in their respective compartments is modeled using the mathematical formalism of Brownian motion with account of the geometrical constraints imposed by the organization of the model stage. A particle is supposed to move in a viscous medium under the action of a random force arising from collisions with molecules of the medium. This processes is modeled with the Langevin equation [59]

$$\xi \frac{dx}{dt} = f(t) \qquad (7)$$

where friction coefficient $\xi = 6\pi\eta a$ (η is viscosity and a is particle radius), $f(t)$ is a random force distributed normally with a zero mean and $2kT\xi$ dispersion.

Equation (7) was solved numerically, with the time step chosen so that the mean displacement of the particle per step was about one-tenth its diameter. Thereby we achieved acceptable accuracy in reasonable computing time. Periodic boundary conditions were imposed on the sides of the stage, and account was also taken of particle bouncing from physical surfaces, including the membrane and protein complexes. Each particle could carry an electron or not (which was visualized as particle color).

The states of complexes, the interaction mechanisms, and the carrier movements were set by certain rules. At the extent of detail used, we can see the following (Fig. 8). The thylakoid membrane delimits the inner space (lumen) where Pc particles move and each can carry an electron. Outside, in the stroma, Fd particles move and also can carry electrons. The membrane is spanned by PS and cytochrome complexes; their concentrations and sizes were chosen from the literature data [56, 57, 60].

The ET mechanism is as follows: if a mobile carrier during chaotic Brownian movement approaches a protein complex to a distance smaller than a certain effective interaction radius, with a certain probability the carrier is docked onto the complex. This radius is a model parameter (the maximal distance at which docking is possible) and was chosen to be equal to the collision distance. The docking probability is also a model parameter. These values can be estimated upon examining the influence of these parameters on the kinetic constants of carrier–complex interaction.

MODELS OF PROTEIN CARRIER INTERACTION

ET between the membrane-embedded complexes involves mobile carriers. In kinetic modeling, the aggregate of these events is described by a single bimolecular reaction. However, the process includes three consecutive steps: (i) Brownian diffusion of the mobile carrier in the compartment; (ii) carrier–complex approach owing to electrostatic attraction, mutual orientation, and formation of a transfer-competent ensemble (docking); (iii) transfer of the electron within this ensemble (tunneling). The arrangement of the *bf*–Pc ensemble is shown in Fig. 9.

Carrier docking to the complex is determined not only by the collision probability but also by their mutual disposition; a prominent part here is played by the local charge interactions.

To model the protein–protein complexing, to predict the structure and assess the binding rate constant, use is often made of Brownian dynamics [61–67]. In this approach, individual proteins are considered solid, their geometry is modeled at atomic resolution, and electrostatic interactions are considered in detail. However, this approach does not allow one to consider ensembles of molecules interacting on or in the membrane. Therefore, we combined Brownian dynamics with direct multiparticle simulation [29–32, 68, 69].

First, protein interaction must be modeled in solution in order to check the adequacy of the basic model and to estimate from the kinetic data the multiparticle model parameters (docking probability and radius). Such models were built by us for cytochrome *f* with Pc [29, 32] and for PS I with stromal Fd [68] and Fld [69]. The molecules were regarded as Brownian particles undergoing translational and rotational motions in a viscous medium under the action of a random force (arising from collisions with molecules of the milieu) and an electrostatic force (included at distances smaller than 35 Å). We made use of the Langevin equation describing the time change in every coordinate caused by these forces.

For the translational motion the equation appears as

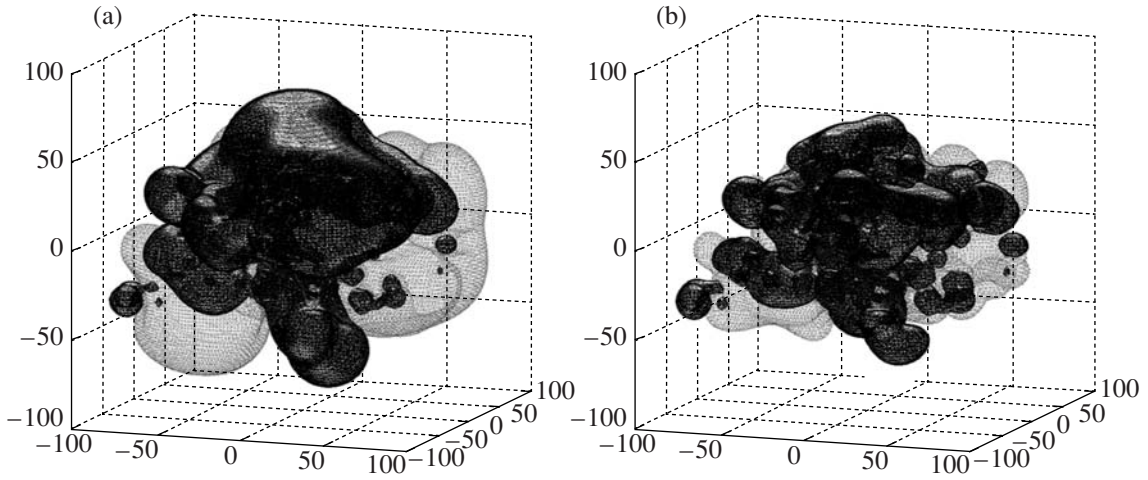

Fig. 10. Equipotential surfaces for PS I (acceptor side up): (gray) –6.5 and (black) 6.5 mV; ionic strength (a) 0 and (b) 80 mM.

$$\xi_t^x \frac{dx}{dt} = f_x(t) + F_x, \quad \langle f_x(t) \rangle = 0,$$
$$\langle f_x(t)^2 \rangle = \frac{2kT\xi_t^x}{\Delta t} \tag{8}$$

where x is the corresponding coordinate, ξ_t^x is the coefficient of viscous friction along this coordinate, $f_x(t)$ and F_x are the projections of the random and the electrostatic forces on the x axis; k is the Boltzmann constant and T is temperature; $F_x = -q\frac{d\varphi}{dx}$, q is charge and φ is the potential.

For the rotational motion we have

$$\xi_r^x \frac{d\varphi}{dt} = m_x(t) + M_x, \quad \langle m_x(t) \rangle = 0,$$
$$\langle m_x(t)^2 \rangle = \frac{2kT\xi_r^x}{\Delta t} \tag{9}$$

where ξ_r^x is the friction coefficient for rotation about the x axis, $m_x(t)$ and M_x are the moments of the random and the electrostatic forces relative to the x axis.

To simplify the calculation of friction coefficients, the Pc and Cyt *f* molecules were represented as ellipsoids of rotation. The 3D model of the molecule was constructed from the PDB data. The ellipsoid size and axes were chosen so that the moments of inertia of the initial molecule and the corresponding ellipsoid coincided under uniform density. For details of calculations, see [31, 70].

To calculate protein collisions, their shapes were described with sets of spheres. The radii and center coordinates of the spheres were chosen so that with a minimal set of spheres the deviation of the resulting shape from the protein surface did not exceed 2 Å (or 1 Å in other series).

A protein approaching other proteins (complexes) orientates in their electric field; as shown by computational experiments, this markedly increases the apparent rate constant relative to that in the case of random contacts.

The PDB data on local charges were used to build equipotential surfaces of the interacting proteins. The force and the moment that the protein experiences in the electrostatic field of other proteins are obtained by summation of the values for all its charges calculated with equations (8)–(9).

The equipotential surfaces calculated for PS I [69] are shown in Fig. 10.

To estimate the parameters of direct models, their results were compared with the experimental data for mutant proteins differing in local charges and hence in the shape of equipotential surfaces. The models yielded experimentally consistent dependences of rate constants for interactions of Cyt *f* with Pc [32, 70] as well as PS I with Fd and Fld [68, 69] on ionic strength for various mutants.

At certain parameter values the model could describe the experimentally observed nonlinear dependence of the protein binding constant on ionic strength. Hence it is sufficient to take into account only electrostatic interactions. The model for solution was also used to study the dependence of the rate constant on the geometry of the reaction volume. It has been demonstrated that a change in geometric dimensions can substantially alter the apparent rate and thus be an efficient mechanism whereby the cell can regulate the photosynthetic processes (for instance, in osmotic stress).

The protein interaction parameters obtained in solution were used to simulate the Pc–Cyt *f* interplay in the thylakoid lumen [31], and particularly examine the dependence of the reaction rate on the lumenal span. As

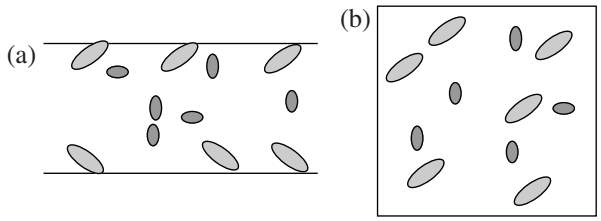

Fig. 11. Two stage versions for numerical experiments: (a) Cyt *f* molecules are membrane-bound in accordance with structural data; (b) all molecules diffuse in a cubic space of the same volume as in (a).

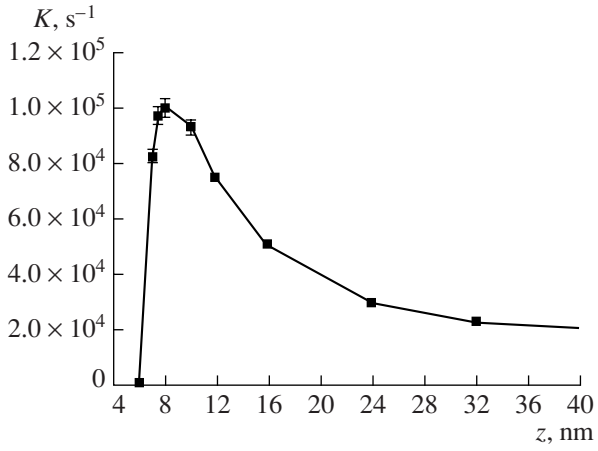

Fig. 12. The rate of Pc-Cyt *f* complexing (normalized to Cyt *f* concentration in the thylakoid) versus the intermembrane distance *z* (at a constant number of molecules).

shown in Fig. 12, the rate is maximal at 8 nm, which corresponds to the intermembrane distance determined during normal photosynthesis. At greater distances the rate declines because of the decreasing Pc concentration. At smaller distances the rate drops because the Pc diffusion in the lumen is hindered and then becomes impossible; this corresponds to the suppression observed in hyperosmotic stress.

CONCLUSIONS AND PROSPECTS

The aggregate of processes in the photosynthetic membrane makes the primary "factory" that provides the living nature with energy. It is a unique object for studying the processes in live systems at the level of subcellular nanostructures. Kinetic ET models (sets of differential equations) have proved quite useful in describing fluorescence induction in different illumination regimes. The kinetic approach may be also effective in relating the primary photosynthetic processes with those of dark metabolism of the plant cell, Calvin cycle, nitrogen and sulfur cycles, etc. [71–73]. The state of these pathways affects the reduction of the quinone pool, the efficacy of the PS I acceptor part, the relation of linear and cyclic ET. In a model relating primary processes with metabolism it is perhaps not expedient to use detailed submodels of multisubunit complexes; simplified modules would suffice provided that they retain the main kinetic characteristics of the full versions. Such models can be applied in analysis of not only the fluorescence rise but also the later parts of the induction curve. It is noteworthy that various kinds of stress (inhibitors, starvation, etc.) substantially alter the shape of the fluorescence curve at times exceeding 1–2 s after switching on the light. These alterations are often connected with the effects of oxygen stress, impairment of protein synthesis, and other processes not yet known in detail. Nonetheless, such processes must be included (be it as parameters) in the models intended for quantitative analysis in biotechnological and ecological monitoring.

The kinetic approach has proved efficient in estimating the reaction rate constants and the relationship of energy fluxes at particular steps of the ET chain. However, ODE sets are poorly applicable to describing the spatial heterogeneity and complicated geometry of the supramolecular photosynthetic machinery. Furthermore, the primary reactions of photosynthesis involve relatively small numbers of molecules (tens or hundreds) within compartments, so the approach based on notions of statistical physics is not quite valid in this case.

To model the interaction of macromolecular ensembles of elaborate shape in a complicated environment, we develop the approach of direct multiparticle modeling, whereby the processes are simulated "just as we see them."

The simulated molecules undergo Brownian motion, mutually orientate in the electrostatic field, and form complexes on a 3D stage built in accordance with our knowledge of the spatial organization of the photosynthetic machinery. The adequacy of the model is checked by correspondence of the calculated kinetic characteristics to the experimental data.

An advantage of direct modeling is the possibility of directly taking into account the shape and size of molecules and elements of the reaction volume. Changing the shape and dimensions of the reaction space, the number and dispositions of the reacting molecules, and other characteristics, we can see their influence on the reaction rate. Using the PDB data, we can directly calculate the distribution of the electric potential around each molecule and assess the role of electrostatic interactions in docking and formation of a competent ensemble prerequisite to the redox reaction. In a kinetic model, such assessment is only possible through additional "effective" parameters, which are then hard to interpret within physical notions. Direct multiparticle simulation makes it possible to understand how the physical mechanisms of molecular interactions (diffusion, electrostatics, etc.) determine the overall dynamics of cell processes.

Currently we are simulating the interaction of PS I in the membrane with the donor Pc in the lumen and the acceptor Fd(Fld) in the stroma. Study of these events within a unified model may shed light on the mechanisms whereby the photosynthetic RC can be regulated by its donor/acceptor environs.

Another direction of research is an attempt to include into the multiparticle model the processes generating the transmembrane proton gradient. We are also working on a model that would integrate the kinetic approach (transfer within complexes described with state probability equations) and direct simulation (ET by mobile carriers).

Light-induced ET starts only after docking, for which the direct modeling has already proved superior. While the physics of events within the RC have to be described with the means of molecular dynamics, kinetic models apparently suffice for intracomplex ET related to fluorescence in native objects.

On the whole, we believe that methods of kinetic and direct multiparticle modeling and their combinations are promising both in the basic research on the living cell and in the practical aspect such as determining the state of the plant cell in biotechnological and ecological monitoring.

REFERENCES

1. G. Yu. Riznichenko, Usp. Nauki Tekhniki, Ser. Biofiz. **31** (1991).
2. G. Y. Riznichenko, G. V. Lebedeva, O. V. Demin, et al., J. Biol. Phys. **25**, 177 (1999).
3. G. Yu. Riznichenko, G. V. Lebedeva, O. V. Demin, et al., Biofizika **45**, 452 (2000).
4. G. Yu. Riznichenko and A. B. Rubin, in *Problems of Reguation in Biological Systems*, Ed. by A. B. Rubin (IKI-RKhD, 2007), pp. 165–194 [in Russian].
5. T. N. Vorobieva, G. Yu. Riznichenko, and K. V. Shaitan, Studia Biophysica **100**, 65 (1984).
6. G. Yu. Riznichenko, T. N. Vorob'eva, and E. N. Khrabrova, Biofizika **31**, 793 (1986).
7. E. N. Khrabrova, T. N. Vorob'eva, and G. Yu. Riznichenko, Biofizika **34**, 429 (1989).
8. G. Y. Riznichenko, T. N. Vorobjeva, and E. N. Chrabrova, Photosynthetica **24** (3), 37 (1990).
9. I. B. Kovalenko, D. M. Ustinin, N. E. Grachev, et al., Biofizika **48**, 656 (2003).
10. G. Renger and A. Shulze, Photochem. Photobiol. **9**, 79 (19851
11. N. G. Bukhov, Kh. G. Damirov, E. G. Dzhibladze, et al., Biol. Nauki **4**, 28 (1986).
12. E. Baake and J. P. Schloder, Bull. Math. Biol. **54**, 999 (1992).
13. J. Eavergne and H.-W. Trissl, Biophys. J. **68**, 2474 (1995).
14. G. V. Lebedeva, N. E. Belyaeva, G. Yu. Riznichenko, A. B. Rubin, and O. V. Demin, Zh. Fiz. Khim. **74**, 1874 (2000).
15. V. P. Shinkarev, Photochem. Photobiol. **67**, 683 (1998).
16. A. D. Stirbet and R. J. Strasser, Archs des Sci. **48**, 41 (1995).
17. A. D. Stirbet and R. J. Strasser, Math. Comp. Simulat. **42**, 245 (1996).
18. A. D. Stirbet, Govindjee, B. J. Strasser, and R. J. Strasser, J. Theor. Biol. **193**, 131 (1998).
19. R. J. Strasser and A. D. Stirbet, Math. Comp. Simul. **48**, 3 (1998).
20. R. J. Strasser and A. D. Stirbet, Math. Comp. Simul. **56**, 451 (2001).
21. R. J. Strasser, M. Tsimilli-Michael, and A. Srivastava, in *Chlorophyll Fluorescence: A Signature of Photosvnthesis*, Ed. by G. Papageorgieou and Govindjee (Springer, Dordrecht, 2004), Vol. 19, pp. 321–362.
22. H.-W. Trissl and J. Lavergne, Austr. J. Plant Physiol. **22**, 183 (1994).
23. H.-W. Trissl, Y. Gao, and K. Wulf, Biophys. J. **64**, 974 (1993).
24. D. Lazar, J. Theor. Biol. **220**, 469 (2003).
25. X.-G. Zhu, Govindjee, N. R. Baker, et al., Planta **223**, 114 (2005).
26. N. E. Belyaeva, V. Z. Pashchenko, G. Renger, G. Yu. Riznichenko, and A. B. Rubin, Biofizika **51**, 976 (2006).
27. G. V. Lebedeva, N. E. Belyaeva, O. V. Demin, G. Yu. Riznichenko, and A. B. Rubin, Biofizika **47**, 1044 (2002).
28. N. E. Belyaeva, Candidate's Dissertation in Physics and Mathematics (MSU, Moscow, 2004).
29. I. B. Kovalenko, A. M. Abaturova, P. A. Gromov, et al., Matem. Komp. Obraz. **12** (3), 955 (2005).
30. I. B. Kovalenko, A. M. Abaturova, D. M. Ustinin, et al., Biofizika **52**, 402 (2007).
31. I. B. Kovalenko, A. M. Abaturova, P. A. Gromov, et al., Biofizika **53**, 261 (2008).
32. I. B. Kovalenko, A. M. Abaturova, P. A. Gromov, et al., Phys. Biol. **3**, 121 (2006).
33. N. E. Belyaeva, V. Z. Pashchenko, G. Renger, Matem. Komp. Obraz. **13**, 333 (2006).
34. M. D. Kamali, G. V. Lebedeva, O. V. Demin, et al., Biofizika **49**, 1061 (2004).
35. S. Malkin, Biochim. Biophys. Acta **234**, 425 (1971).
36. E. M. Sorokin, Fiziol. Rast. **20**, 733 (1973).
37. A. B. Rubin and V. P. Shinkarev, *Electron Transport in Biological Systems* (Nauka, Moscow, 1984) [in Russian].
38. G. Sh. Vashakhmadze, Kh. G. Damirov, I. R. Vasil'ev, et al., Biol. Nauki **5**, 42 (1985).
39. T. N. Vorob'eva, G. Yu. Riznichenko, A. B. Rubin, et al., Mol. Biol. **20**, 1203 (1986).
40. S. K. Chamorovskii, E. N. Khrabrova, and G. Yu. Riznichenko, Biofizika **35**, 16 (1990).
41. W. J. Vrcdenberg, Biophys. J. **79**, 26 (2000).
42. N. E. Belyaeva, G. V. Lebedeva, O. V. Demin, et al., Matem. Komp. Obraz. **11**, 765 (2004)
43. N. E. Belyaeva, V. Z. Pashchenko, G. Renger, et al., Matem. Komp. Obraz. **13**, 333 (2006).
44. G. Hauska and M. Arnold, in *Probing Photosynthesis*, Ed. by M. Yunus, U. Pathre, and P. Mohanty (Taylor and Francis, London, 2000), pp. 109–126.
45. A. B. Hope, Biochim. Biophys. Acta **1456**, 5 (2000).

46. A. A. Bulychev and W. J. Vredenberg, Bioelectrochemistry **54**, 157 (2001).
47. H. Dau and K. Sauer, Biochim. Biophys. Acta **1102**, 91 (1992).
48. C. Zheng, M. E. Davis, and J. A. McCamrnon, Chem. Phys. Lett. **173**, 246 (1990).
49. K. Krab, H. S. Van Walraven, M. J. S. Schoolts, et al., Biochim. Biophys. Acta **809**, 236 (1985).
50. I. A. Reynolds, E. A. Johnson, and Tanford, Proc. Natl. Acad. Sci. USA **82**, 6869 (1985).
51. O. V. Demin, H. W. Westerhoff, and B. N. Kholodenko, Biokhimiya **63**, 755 (1998).
52. N. E. Belyaeva, G. V. Lebedeva, and G. Yu. Riznichenko, Matem. Komp. Obraz. **10**, 263 (2003).
53. D. G. Nicholls, Eur. J. Biochem. **50**, 305 (1974).
54. I. I. Potossin and G. Schonknecht, J. Membr. Biol. **152**, 223 (1996).
55. O. Van Kooten, J. F. H. Snel, and W. J. Vredenberg, Photosynth. Res. **9**, 211 (1986).
56. P. A. Albertsson. Recent Res. Devel. Bioener. **143** (2000).
57. P. A. Albertsson, Trends Plant Sci. **6**, 349 (2001).
58. I. B. Kovalenko, D. M. Ustinin, M. V. Serdobol'skaya, et al. in *Proc. VIII Internat. Conf. "Nonlinear World"* (Astrakhan, 2004), pp. 223–229.
59. A. Kh. Vorob'ev, *Diffusion Problems in Chemical Kinetics* (Izd. MGU, Moscow, 2003) [in Russian].
60. R. Malkin and K. Niyogi, in: *Biochemistry & Molecular Biology of Plants*, Ed. by B. Buchanan, W. Gruissem, and R. Jones (Kluwer, Dordrecht, 2000), pp. 413–429.
61. E. L. Gross, Biophys. J. **87**, 2043 (2004).
62. E. L. Gross and D. C. Pearson, Biophys. J. **85**, 2055 (2003).
63. E. L. Gross and I. Roscnbcrg, Biophys. J. **90**, 366 (2006).
64. E.J. Haddadian and E. L. Gross, Biophys. J. **88**, 2323 (2005).
65. E.J. Haddadian and E. L. Gross, Biophys. J. **91**, 2589 (2006).
66. D. C. Pearson and E. L. Gross, Biophys. J. **75**, 2698 (1998).
67. G. M. Ullmann, E.-W. Knapp, and N. M. Kostic, J. Am. Chem. Soc. **119**, 42 (1997).
68. A. N. D'yakonova, I. B. Kovalenko, A. M. Abaturova, et al, Matem. Komp. Obraz. **15** (3), 79 (2008).
69. A. M. Abaturova, I. B. Kovalenko, G. Yu. Riznichenko, et al., Matem. Komp. Obraz. **15** (3), 71 (2008).
70. I. B. Kovalenko, A. M. Abaturova, P. A. Gromov, et al., Matem. Komp. Obraz. **13** (3), 323 (2006).
71. V. A. Karavaev and A. K. Kukushkin, Biofizika **38**, 958 (1993).
72. S. A. Kuznetsova and A. K. Kukushkin, Biofizika **41**, 1247 (1996).
73. T. T. Nguen, T. A. Karelina, and A. K. Kukushkin, Biofizika **52**, 861 (2007).